Chapter 2

Detector for the Linear Collider

General Detector Concepts and Detector Performance

Conveners: M. Martinez, D.J. Miller, M. Piccolo

Working Group: A. Andreazza, M. Battaglia, G. Blair, G. Daskalakis, A. Juste, A. Kyriakis, C. Markou, H.U. Martyn, H. Nowak, I. Riu, M. Sachwitz, H.J. Schreiber, D. Schulte, R. Settles, R. Shanidze, C. Shepherd-Themistocleous, S. Shichanin, E. Simopoulou, R. Vuopionperä, C. Troncon

Detector Subsystems

Conveners: M. Mazzucato, D. Saxon, R. Settles

Working Group: S. Aïd, A. Andreazza, P. Bambade, T. Barklow, W. Bartel, M. Battaglia, R. Bellanzzini, S. Bertolucci, G. Blair, R. Brinkmann, I. Brock, R. Brown, J. Bürger, P.J. Bussey, M. Caccia, P. Checchia, G. Coignet, P. Colas, P. Clarke, C. Damerell, M. David, A. De Roeck, E. Elsen, E. Fernandez, Y. Giomataris, T. Greenshaw, R. Heuer, C. Heusch, N. Holtkamp, P. Hüntemeyer, P. Janot, L. Jönsson, F.P. Juster, B.J. King, F. Kircher, V. Korbel, U. Kötz, Y. Kurihara, P. Le Du, M. Leenen, W. Lohmann, C. Luci, L. Mandelli, M. Martinez, C. Meroni, J. Meyer, D. Miller, R. Nahnhauer, O. Napoly, R. Nania, R. Orava, M. Piccolo, M. Pohl, D. Reed, F. Richard, A. Rousarie, H.-G. Sander, U. Schneekloth, H.J. Schreiber, S. Schreiber, D. Schulte, C. Shepherd-Themistocleous, F. Simonetto, K. Sinram, A. Skillman, A. Sopczak, P. Steffen, H. Steiner, J. Steuerer, G. Tonelli, M. Tonutti, C. Troncon, C. VanderVelde, G. Vegni, A. Wagner, N. Walker, M. Weber, W. Wiedenmann, G.W. Wilson, K. Zapfe-Düren

Collider-Experiment Interface

Conveners: N. Holtkamp, M. Leenen, O. Napoly

Working Group: G. Bardin, R. Brinkmann, C. Cavata, S. Drozhdin, J.-P. Jorda, N. Mokhov, M. Sachwitz, H.J. Schreiber, S. Schreiber, D. Schulte, R. Settles, K. Sinram, N. Walker, K. Zapfe-Düren

Contents

2.1 General Detector Concept

2.1.1 Introduction

A detector for e^+e^- experiments up to the highest linear collider energies is presented here. It results from one set of choices among many possibilities considered during the *ECFA/DESY Study on Physics and Detectors for the Linear Collider* [1]. As will be shown the detector matches the requirements of the physics analyses and could essentially be built today. The performance of all subsystems can be improved with further R&D, which is also discussed.

Requirements

The physics programme of the linear collider has been the subject of intense investigation in the present [1] and past [2]–[14] studies. A few example experiments listing the analysis aspects needing excellent performance ($\surd$) show that the detector has to meet high demands on quality:

	DETECTOR				
PHYSICS	Missing Energy	Jet-jet Reconstruction	Lepton I.D.	b,c,τ Vertexing	Forward Direction
Higgs branching ratios	$\surd$	$\surd$	$\surd$	$\surd$	$\surd$
Top threshold scan	$\surd$	$\surd$		$\surd$	$\surd$
W-boson couplings	$\surd$	$\surd$	$\surd$		$\surd$
$\tilde{\chi}_j^\pm \tilde{\chi}_i^0 \tilde{\ell} \tilde{q}$ spectroscopy	$\surd$	$\surd$	$\surd$	$\surd$	

The most essential performance goals for the detector can be summarized as follows:

- Excellent vertex resolution for heavy flavour identification (b, c, τ vertexing).
- Tracking with accurate momentum determination and high redundancy to handle easily the multijet environment (jet-jet reconstruction).
- Good energy-flow measurement given by high granularity in the calorimeters and particle identification in the tracking (jet-jet reconstruction, missing energy).
- Hermetic, with good measurement in the forward direction (missing energy, forward direction).
- Very good lepton identification and e-π separation (lepton identification).
- Flexible trigger – because of possible backgrounds (see below).

Table 2.1.1 lists the major differences in a detector for the linear collider as compared to LEP2.

Difference LEP 2→LC	Possible Improvements to Detector
Smaller beam pipe	Instrumentation down to smaller radius with detectors having higher resolution
Higher multiplicities, more beam-associated background	Pixels essential in vertex detector; minimize mass in whole tracking volume; higher B field
Higher peak track energies (especially leptons)	Better point resolution; more measured points; higher B field
Higher e and γ energies	Thicker electromagnetic calorimeter ECAL
Higher hadron energies	Thicker hadronic calorimeter HCAL
Narrower and/or more jets	Better jet reconstruction; fine granularity; better HCAL; ECAL and HCAL inside coil

Table 2.1.1: *Differences between detectors for LEP and the LC.*

Good vertex resolution is demanded because much of the new physics to be studied involves heavy flavors, especially Higgs and top decays. Only with the best vertex resolution will it be possible to measure charm signals well, so that the beam pipe radius should be as small as possible.

LEP experience has shown how cleanly signals can be recognized and separated by using the redundant information from a many-layered tracker. Even dense high-energy jets can be resolved into individual particles, and at the linear collider this must be possible in the presence of a large number of isolated photon hits. The tracks of primary events must be identified in the main tracker and followed back into the vertex detector. The vertex detector with at least three layers will allow stand-alone tracking to match with the tracks found in the main tracker.

Many of the physics channels for SUSY, top and W^+W^- involve significant amounts of missing energy. The detector has to be hermetic to identify these events. The shielding mask around the mini-beta quadrupoles is a feature specific to the LC. R&D work is needed to develop a way of measuring the energy deposited in it.

The higher energy of the LC will either produce more energetic and narrower jets than LEP (e.g. in W^+W^- production) or events with many more jets to be resolved and measured (e.g. in top-antitop or the production of pairs of SUSY Higgs bosons). It will be essential to measure individual jet energies in order to establish the detailed energy flow for all parts of the event. This involves the measurement of charged tracks and the subtraction of the associated energy from the observed neutral clusters. Fine granularity is needed in both the electromagnetic and the hadronic calorimeter. The major part of all showers must be measured before they reach the coil, which spreads the

Vertexing	$\delta(IP_{r\phi}) \leq 10\,\mu m \oplus \frac{30\,\mu m\ \mathrm{GeV}/c}{p\sin^{3/2}\theta}$ $\delta(IP_z) \leq 20\,\mu m \oplus \frac{30\,\mu m\ \mathrm{GeV}/c}{p\sin^{5/2}\theta}$
Forward Tracking	$\frac{\delta p}{p} < 20\,\%$, $\delta_\theta < 200\,\mu\mathrm{rad}$ for 100–250 GeV particles down to lowest polar angle θ.
Tracking	$\frac{\delta p_t}{{p_t}^2} \leq 1 \cdot 10^{-4} (\frac{\mathrm{GeV}}{c})^{-1}$ Good particle identification.
Electromagnetic Calorimeter	$\frac{\delta E}{E} \leq 0.10 \frac{1}{\sqrt{E}} \oplus 0.01$ (E in GeV) Granularity $0.9^\circ \times 0.9^\circ$, at least 3 samples in depth.
Hadronic Calorimeter	$\frac{\delta E}{E} \leq 0.50 \frac{1}{\sqrt{E}} \oplus 0.04$ (E in GeV) Granularity $2^\circ \times 2^\circ$, at least 3 samples in depth.
Muon Detector	Fe yoke instrumented as tail catcher and muon tracker. Toroid momentum analysis for forward muons ($\theta < 15^\circ$), $\frac{\delta p}{p} < 20\,\%$.
Energy Flow	$\frac{\delta E}{E} \simeq 0.3 \frac{1}{\sqrt{E}}$ (E in GeV)
Hermetic Coverage	$\lvert\cos\theta\rvert < 0.99$

Table 2.1.2: *Detector performance goals.*

clusters and degrade the energy resolution. The LEP detectors are presently gaining experience in handling multijet events at higher energies, and the difficulty of this undertaking is reflected in the emphasis on very good jet resolution for the LC detector.

2.1.2 Layout Concept

The performance goals given in Tab. 2.1.2 are derived from the needs of the physics analysis and match the technical feasibility. The basic layout follows the well-proven concept of tracking in a magnetic field at inner radii and calorimetry at outer radii. Two alternatives were considered: (i) a detector with large solenoid and calorimetry inside the coil and (ii) a compact detector with small solenoid and calorimetry outside the coil. The large detector was chosen in order to achieve better jet resolution and because of the good experience with such detectors at LEP/SLC/HERA.

Figure 2.1.1 shows a schematic cross section through the detector and Fig. 2.1.2 some details of the inner region. Table 2.1.3 gives the subdetector techniques chosen and Tab. 2.1.4 the the subdetector dimensions.

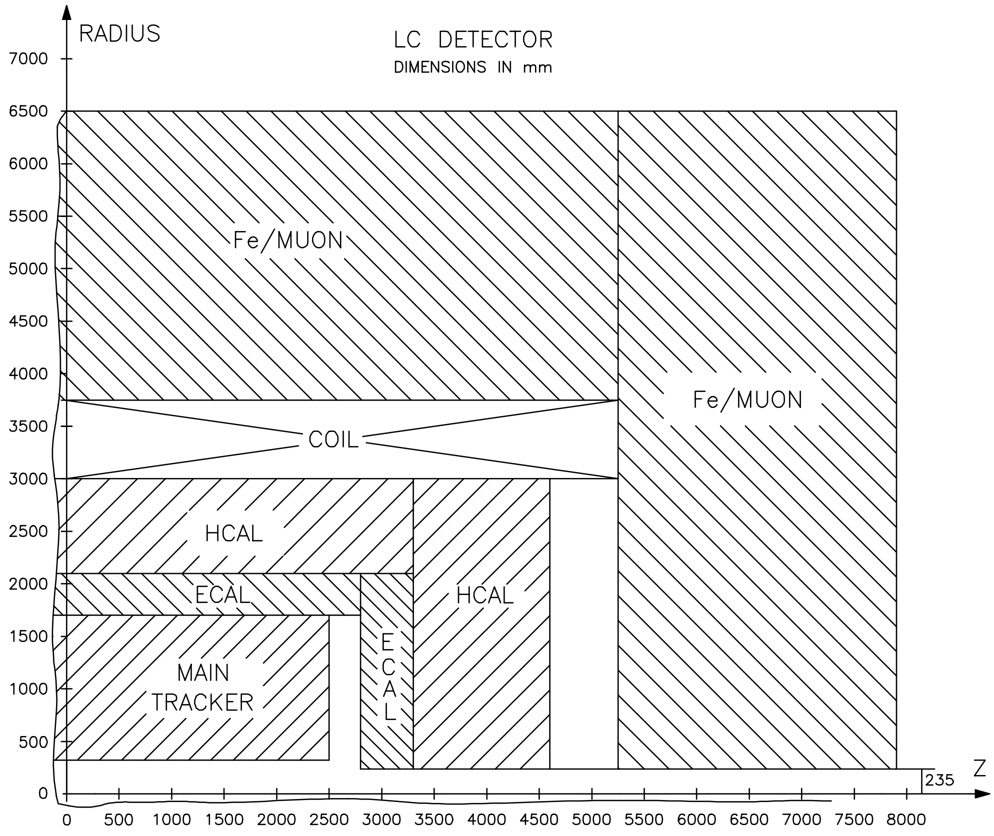

Figure 2.1.1: *Schematical layout of one quadrant of the LC Detector.*

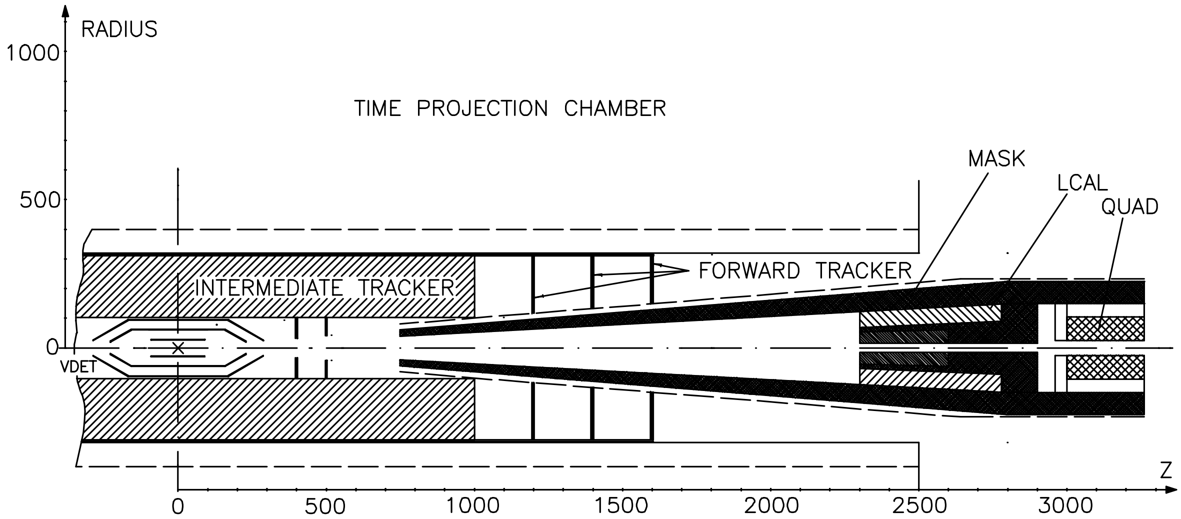

Figure 2.1.2: *Schematic layout of the inner region of the detector.*

Subdetector	Technique chosen (Radiation Lengths)	Alternative techniques
	Barrel	
Beam pipe	($0.3\,\%\ X_0$)	
Vertex detector	CCD or APS ($1.6\,\%$ or $2.4\,\%\ X_0$)	Silicon strip
Intermediate tracker	Honeycomb straw tubes ($0.23\,\%\ X_0$)	Scintillating fibers with drift chamber; Silicon strip
Intermediate layer	Double-sided silicon strip ($1\,\%\ X_0$)	
Main tracker	Time projection chamber ($3\,\%\ X_0$ to outer field cage)	MSGC; Silicon strip
(Total thickness to outermost tracking radius = $6.1\,\%$ (CCD) or $6.9\,\%$ (APS) X_0)		
Presampler	Scintillating fibers	
E-M calorimeter	Pb-scintillator Shashlik cal.	Spaghetti calorimeter; Crystals
Hadron Calorimeter	Cu-scintillator Shashlik	
Tailcatcher, muon identifier	Resistive plate chambers	Limited streamer
	Forward	
Luminosity calorimeter	Scintillating fibers in Pb	Spaghetti calorimeter Silicon-tungsten Shashlik
Instrumented mask	Quartz fibers in W	
Forward tracker	Silicon strip and/or pixels	
Forward muon tracker	Toroids with honeycomb tubes	

Table 2.1.3: *Techniques chosen for the LC detector.*

Subdetector	Radial extent		Longitudinal extent	
	r_{min} [mm]	r_{max} [mm]	$\lvert z_{\mathrm{min}}\rvert$ [mm]	$\lvert z_{\mathrm{max}}\rvert$ [mm]
Beam pipe		20		
Vertex detector	25	100		300
			(including endcaps)	
Forward tracker discs			at 400, 500, 1200, 1400, 1600	
Intermediate tracker	120	300		1000
Intermediate Si layer	300	320		1600
Main Tracker (TPC)	320	1700		2800
Sensitive volume	386	1626		2500
ECAL Barrel	1700	2100		2800
ECAL Endcap	235	2100	2800	3300
HCAL Barrel	2100	3000		3300
HCAL Endcap	235	3000	3300	4600
Coil Cryostat	3000	3750		5250
Iron Barrel	3800	6400		5250
Iron Endcap	235	6400	5250	7900
Toroid	400	3000	7900	9400
	Angular range			
	θ_{min} [mrad]	θ_{max} [mrad]		
TESLA Mask	55	80	750	2800
(conical part)	r_{outer}=62 to 225 mm			
SBLC Mask	85	125	750	1800
(conical part)	r_{outer}=62 to 225 mm			
TESLA $\mathcal{L}$cal	30	55	2300	2800
SBLC $\mathcal{L}$cal	30	85	1300	1800

Table 2.1.4: *Dimensions of the LC subdetectors.*

Detector Choices

The techniques chosen for the different subdetectors (Tab. 2.1.3) are reviewed briefly in the following paragraphs and compared with the alternative techniques. The full discussion follows in Section 2.2.

Either Charged Coupled Devices (CCD) or Active Pixel Sensors (APS) could provide the performance required for a vertex detector. They are regarded as alternatives at this stage, with R&D programmes continuing. Both are described in Section 2.2.1 below. The advantages of CCDs are their uniformly small pixel size ($20\,\mu\text{m}^2$, compared with $50\,\mu\text{m}^2$ for APSs) and their thinness ($30\,\mu$m of silicon with very light support structures, giving only $0.12\,\%X_0$ per layer, as compared with $0.8\,\%X_0$ for APS). APSs are presently better matched to the time structure of the machine (though current development of fast-clear facilities will help the CCDs to compete) and are more resistant to the neutron radiation. Silicon strip detectors are shown not to be suitable for the vertex detector because they would have occupancy problems with high multiplicity events and the photon background in the innermost layers. The outer two layers of the vertex detector will taper down conically at $30°$ at the outer edge of the barrel.

The intermediate tracker needs good position resolution in $r\phi$ to aid linking tracks from the main tracker to the vertex detector, and it also provides the fast track-trigger. Both straw tubes and scintillating fibers have been investigated. The straw-tube "honeycomb chamber" was chosen as having the advantage of better intrinsic resolution and much less material ($0.23\,\%\ X_0$ compared with $1\,\%\ X_0$ per layer for scintillating fibers). The thin walls in the forward direction represent also an important reduction of material for the forward tracking.

An intermediate Si-strip layer provides a precise reference for connecting the intermediate tracker and vertex detector coordinates with those of the TPC system, and it improves the momentum resolution.

The TPC main tracker has a number of advantages over other techniques. It presents the minimum possible amount of material for the conversion of outgoing photons from beam-beam effects ($3\,\%\ X_0$ for the inner field cage plus gas, compared with $10\,\%$ distributed over the whole volume for MSGCs). Its z resolution is better than a jet chamber, and it can be gated to eliminate the distortion due to positive ions from the detector planes drifting into the detector volume.

For the electromagnetic calorimeter, ECAL, the Pb-scintillator Shashlik technique has been chosen since it gives better 3D granularity than a crystal calorimeter. Crystals would give better energy resolution but physics studies have shown that $\lesssim 10\,\%\sqrt{E}$ will be sufficient. Liquid argon would involve large cryostats which would reduce the space for all inner tracking detectors and introduce cracks which compromise the hermeticity. Also being studied studied is a scintillating fiber presampler, with thin layers of lead converter, which will give precise coordinates for shower conversions; detailed simulations are needed to be sure that this will not compromise the overall resolution of the ECAL. The performance goal for the electromagnetic energy resolution (good performance is needed e.g. for measuring the $H \to \gamma\gamma$ branching ratio) does not allow compensation at hardware level for the measurement of hadronic showers, and good granularity enables this to be done in the off-line software.

Also for the hadron calorimeter, HCAL, a Shashlik approach similar to that for the electromagnetic layer but with copper as absorber, has been chosen, with flexibility to optimize the granularity and the sampling in depth and to match the towers to those of the ECAL. There will be at least five interaction lengths of calorimeter within the coil at the equator, with more in the forward and backward towers.

The tail-catcher will use the iron return-yoke of the magnet to measure the leakage of energy which escapes from the back of the hadron calorimeter and through the coil. A powerful muon detector will also result from sampling the muon tracks in the iron. Resistive plate chambers are likely to be cheaper and easier to build than limited streamer tubes for the same performance. Either technique can also provide fast triggering for cosmic ray events.

The luminosity calorimeter, covering from about 30 to 55 (30 to 85) mrad for TESLA (SBLC) from the beam direction inside the tungsten shielding masks, has to measure high energy electron showers – in the presence of intense soft electromagnetic radiation from beam-beam pair production and beamsstrahlung. It is not yet clear how long scintillators or silicon pad detectors would survive under these circumstances. A solution based on Pb with liquid scintillator in quartz fibers is being studied.

The possibility is being studied of instrumenting the tungsten mask with embedded longitudinal quartz fibers in order to obtain the best possible hermeticity. It remains to be verified that the masking function can be maintained in this case.

A sequence of forward tracking detectors will be used to measure tracks close to the outer surface of the mask, especially muons and Bhabha electrons (for acollinearity measurement to give the luminosity spectrum). Discs of pixel and silicon-strip detectors will be inserted inside the intermediate tracker and inside the TPC inner cylinder.

Forward toroids are needed to measure the sign and the momentum of muons at small angles to the beam direction – e.g. in the study of W^+W^- production or for the absolute c.m.s. energy determination. Strawtube honeycomb chambers before and after the toroids would measure the positions and the bending of muons over a range of angles from 35 to 240 mrad from the beam direction. Beyond that, the muons can be tracked and measured in the iron of the yoke.

2.1.3 Layout for Other Machine Options

e^-e^-, $e^-\gamma$, and $\gamma\gamma$Colliders. This report is largely concerned with the initial phase of the programme of a linear collider, running in the e^+e^- mode. There are three important additional modes of operation which would extend the physics potential, as explained in Chapter 1: e^-e^- collisions and the Compton-collider with its $e^-\gamma$ and $\gamma\gamma$

modes. The luminosity in all three cases will be reduced by a factor of between 1/2 to 1/5 from the e^+e^- luminosity. The detector described in this report will do equally well for e^-e^- studies.

Much more special preparation will be needed to provide the backscattered laser facility for $e^-\gamma$ and $\gamma\gamma$ physics. The linac optics of the final focus region need to be optimized in a different way, access must be provided for the intense laser beams and the beam-crossing angle at intersection must be large enough for radiation and pairs from the conversion points to escape past the focusing quadrupoles. It is therefore anticipated that a second interaction point will need to be provided for $e^-\gamma$ and $\gamma\gamma$ collisions, with a different beam delivery section and its own detector. Because the physics channels to be studied in $e^-\gamma$ and $\gamma\gamma$ are not so different from those in e^+e^- [20], most features of the detector could be similar to those described in this report. The essential difference will be in the region of the conical mask around the beam direction. In order to make room for laser optics the mask will have to come out to larger angles – 150 to 200 mrad, compared with 80 to 100 mrad in the detector described here – and the region inside the mask may not have any room for small-angle calorimetry.

Two Interaction Regions. It may be argued that a second interaction region for e^+e^- studies, with its own detector, should be planned as part of the basic linear collider programme, to provide for scientific redundancy, to have complementary detectors, to give competition between alternating teams, or to insure against failure of a single detector. If provision is made for such a second IR in the collider layout plans, then the needs of $e^-\gamma$ and $\gamma\gamma$ must be borne in mind. The detector in such a second region might well be used for all four collider modes, e^+e^-, e^-e^-, $e^-\gamma$, and $\gamma\gamma$. It should be noted, however, that at a linear collider, contrary to storage rings with more than one experiment, the total available luminosity would have to be shared between the experiments.

2.1.4 The Detector Magnet

The magnetic field has two important rôles: it bends charged particles for momentum measurement and it limits beam related background by imposing a cutoff in the transverse momentum of those e^+e^- pairs from beamstrahlung that enter the detector (see Fig.2.4.9).

In order to reduce the beam-pipe diameter, the aperture of the mask, and the background in the detector, a field of at least 2 T is necessary. With higher fields, the pair background in the vertex detector can be further reduced and the momentum measurement by the tracking further improved. Therefore, a field strength of $B = 3\,\mathrm{T}$ was chosen as being a reasonable compromise between high field, large volume and safe technology.

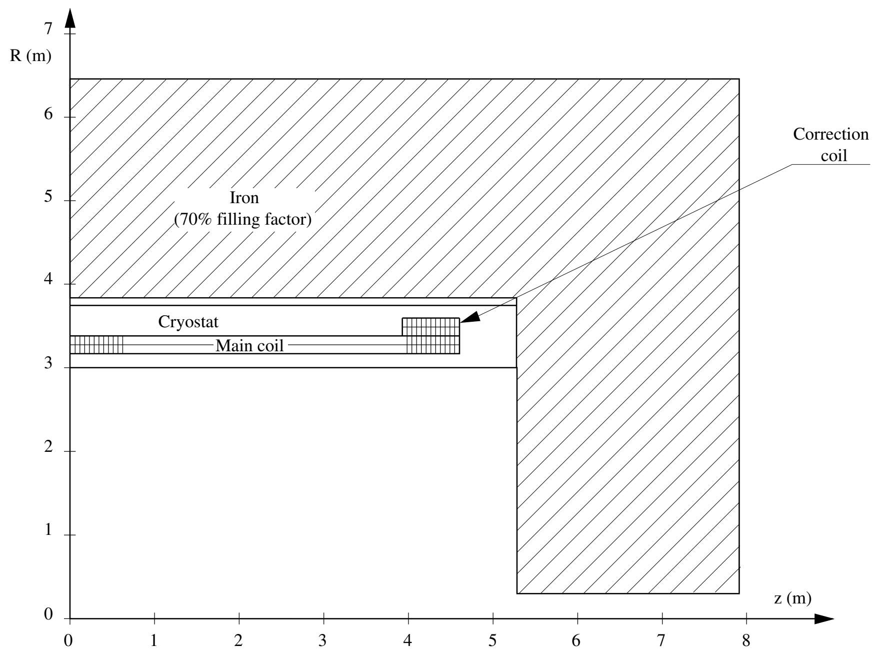

Figure 2.1.3: *Cross section through the magnet.*

The dimensions of the coil are determined by the need to have good momentum resolution and the decision to have the electromagnetic calorimeter and part of the hadronic calorimetry inside the coil. This leads to the choice of an internal coil diameter of 6.0 m. In order to provide good tracking down to $|\cos\theta| = 0.99$, good field homogeneity is required for the TPC in order to reduce $E \times B$ distortions on the electron drift. Thus the length of the magnet was chosen to be 9.2 m.

With these magnet dimensions the last quadrupole doublets are inside the coil. These doublets are superconducting in the case of TESLA, and the 3 T from the main coil is close to but still within a safe margin of their critical field strength.

The large aperture superconducting solenoid selected for this detector is a magnetic configuration which has been used in several previous projects as well as in projects under design. It is more expensive than a compact solenoid would be, but the physics benefits of putting the main calorimetry inside the coil are worth the extra cost. Even with extensive R&D it would not be possible to reduce the thickness of a compact coil to much less than half of a radiation length which would reduce the performance of the calorimeter.

The cross section of the magnet with its iron is shown in Fig 2.1.3. The iron is used both as a magnetic return yoke and as a hadronic tail-catcher and muon filter as described in Section 2.2.6. Table 2.1.5 summarizes the main parameters of the magnet preliminary design.

Dimensions	
Cryostat inner radius (m)	3
Main coil inner radius (m)	3.15
Main coil outer radius (m)	3.35
Correction coil inner radius (m)	3.35
Correction coil outer radius (m)	3.55
Cryostat outer radius (m)	3.75
Iron inner radius (m)	3.8
Iron outer radius (m)	6.4
Iron filling factor (%)	70
Main coil length (m)	9.2
Cryostat overall length (m)	10.5
Magnetic field	
Central field (T)	3
Maximum field at conductor (T)	3.8
Stored energy (MJ)	1 350
Nominal current (A)	15 000
Ampere turns main coil	$21.9 \cdot 10^6$
Ampere turns correction coil	$1.8 \cdot 10^6$
Conductor	
Type	NbTi cable in high purity Al plus mechanical reinforcement
Strand diameter (mm)	1.1
Cu to Sc ratio	1.3
No. of strands in cable	32
Overall dimensions (mm^2)	100×12
Critical current at 4.2 K and 4 T (A)	35 500

Table 2.1.5: *Main characteristics of the superconducting solenoid.*

	BaBar	LHC	LC
Bunch crossing time	4 ns	25 ns	4-708 ns
Level-1 accept rate	2 kHz	100 kHz	<0.1 kHz
Event building	0.4 Gbit/s	20-500 Gbit/s	1 Gbit/s
Processing power	10^3 MIPS	10^6 MIPS	10^5 MIPS

Table 2.1.6: *Comparison of three triggering projects.*

The mechanical and magnetic characteristics of this solenoid lie between those of ALEPH [21] and CMS [22]. Its design will include several features used for these two magnets:

- a high purity aluminum-stabilized conductor, with mechanical reinforcement;
- a compact impregnated winding, with indirect cooling provided by circulating helium at 4.5 K;
- a quench-back protection scheme.

Special features for this magnet are the use of a rather large conductor in order to limit the number of layers to two and the use of correction coils (as in ALEPH) to attain a field homogeneity of better than $\sim 10^{-3}$ in the TPC volume. More details about the design of this solenoid can be found in Ref. [23]. Further optimization of its dimensions will result from studies that follow.

2.1.5 Rates

Trigger and Data Acquisition Overview

This section outlines a functional overview of the event selection and data acquisition (DAQ) systems compatible with both machine proposals (TESLA and SBLC). The trigger structure and data flow are shown in Fig. 2.1.4. At the design luminosity and $\sqrt{s} = 500\,\mathrm{GeV}$, the physics rate to be recorded is expected to be about 0.1 Hz. Backgrounds expected to be rejected by the trigger include those from beam-beam effects (see next Section), beam-gas interactions and cosmic rays. There must be flexibility for adjusting the trigger rate due to background to the needs of the experiment (as is the case at LEP for example).

Extrapolation from previous or recent e^+e^- detectors (LEP detectors and BaBar) as well as advanced studies for LHC experiments allows a realistic model to be proposed based on a two-level scheme that satisfies the basic requirements. Compared to the LHC requirements, the data acquisition for the experiment is not a critical issue (see Tab. 2.1.6)

The DAQ system (see Section 2.2) must deal with

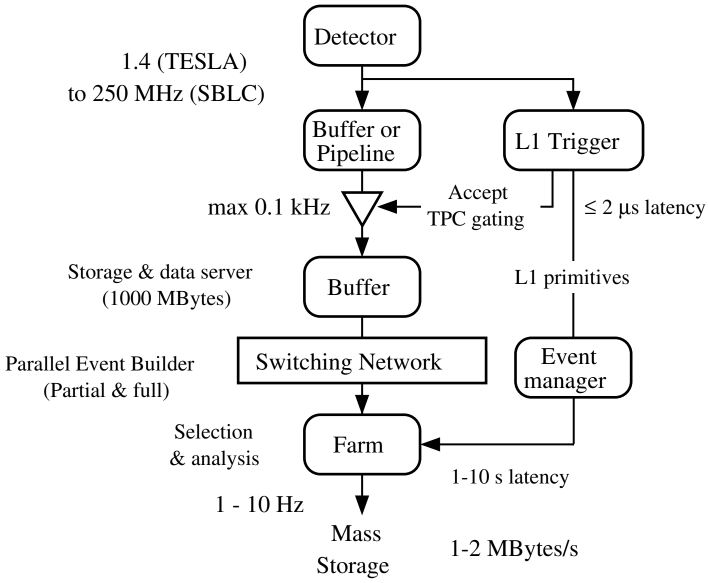

Figure 2.1.4: *Trigger and readout scheme.*

- $2{\cdot}10^7$ ($7{\cdot}10^8$) pixels of APS (CCD) vertex detector which are multiplexed into a few hundred readout channels,
- 10^3 channels of intermediate tracker,
- 10^7 pixels and strips for the forward tracker and intermediate silicon strip layer to be multiplexed into a few hundred channels,
- $7{\cdot}10^8$ TPC pixels read out in 720 k pad channels which will be reduced by multiplexing to a few thousand readout channels,
- 342 k calorimeter readout cells before multiplexing,
- and 200 k muon channels before multiplexing.

The final size of a physics event after zero suppression will be a few hundred kBytes up to about a MByte; the size of background events will be an order of magnitude smaller.

The Level-1 trigger would be adapted to the machine beam/bunch-crossing rate seen in Tab. 2.1.7. A first reduction of the initial background rate to less than 100 Hz can be achieved by fast logic that retains only those events that satisfy simple geometrical, energy deposition or track criteria, as well as pattern matching between subdetectors. Selection algorithms are performed synchronously within $2\,\mu$s latency using a separate stream of coarse dedicated data. Following a Level-1 Accept signal, about 1 GByte/s of front-end raw digitized information produced by the different subdetectors are transferred in parallel to a series of "readout buffers" acting as temporary data storage and server during the next steps of the selection process. Only that level would be affected by the choice of the machine (latency and front-end electronics design). After each Level-1 accept, the TPC signals are digitized during the $50\,\mu$s drift time, introducing a negligible dead time given sufficient front-end buffering. Several techniques will be envisaged, such as triggering the TPC grid at the Level-1 accept rate, or working in a free-running mode if the positive-ion effects in the TPC volume are under control.

Downstream of the Level-1, the second step may combine the event selection and analysis together by using a sequential strategy guided by the Level-1 primitives and trigger flags. At each step, only the event data which is necessary to make a decision is acquired and analyzed. The full event reconstruction (using all calibration constants) is performed only when required for physics analysis. A modern view for an implementation consists of a system with only four standard components: the "sources" data buffers (total capacity of 1000 MBytes), a 1 to 5 Gbit/s network for both protocol and data, the "destination" processing farm (10^5 MIPS) and the event control flow system. The recent development and availability of modern commercial switching network technologies such as ATM already solve the event building aspect, decreasing the complexity of connection and control protocols. Finally, some parameters such as the computing power, the latency and temporary storage buffer size will no longer be critical due to rapid development within the computing industry. After the on-line analysis, a few MBytes/s of data (about 1 % of an LHC typical bandwidth) will be recorded on permanent storage.

Backgrounds

The sources of background, discussed in detail in Section 2.4, are beam-beam effects, synchrotron radiation and debris from the final quadrupoles, and muon backgrounds arising from upstream sources. The main backgrounds are due to beam-beam effects. Table 2.1.7 gives an overview of some machine properties and related background rates.

The bunch crossing time for the two machine options are 6 ns (SBLC) and 708 ns (TESLA) for $\sqrt{s} = 500\,\mathrm{GeV}$. Via the beam-beam interaction, each bunch crossing occurring within the time resolution of the detector may produce particles that can partially obscure a real physics event triggered by a different bunch in the train. The row labeled "Minijet ev./100 ns, $p_T^{\mathrm{min}} = 3.2\,\mathrm{GeV}/c$" gives a measure of the probability of having stiff particles from underlying hadronic events in a good physics event for a typical subdetector with a timing resolution of 100 ns. The last rows show the rates for several physics channels.

	TESLA	SBLC	TESLA	SBLC
[Units in brackets]	0.5 TeV		0.8 TeV	
Beam properties				
Trains/s	5	50	3	50
Bunches/train	1130	333	1130	125
Interbunch spacing	708 ns	6 ns	566 ns	4 ns
$N_{e^\pm}$ per bunch $[10^{10}]$	3.6	1.1	3.6	1.2
$N_{\mathrm{beamstr.}\gamma}$ per $e^\pm$	2.0	1.4	2.4	1.6
$\langle E_{\mathrm{beamstr.}\gamma}\rangle$ [GeV]	3.0	4.7	8.7	11.1
Backgrounds/bunch				
$N_{\mathrm{beamstr.}e^\pm}$/bunch crossing $\theta > 150\,\mathrm{mrad}$, $p_t > 20\,\mathrm{MeV}/c$	31	7	47	17
Hadr.ev./bunch $E_{\gamma\gamma-\mathrm{c.m.s.}} \geq 5\,GeV$	.13	.04	.46	.17
Minijet ev./bunch $[10^{-2}]$ $p_T^{\min} = 3.2\,\mathrm{GeV}/c$	.30	.10	1.6	.66
Backgrounds/100 ns				
$N_{\mathrm{beamstr.}e^\pm}$/100 ns $\theta > 150\,\mathrm{mrad}$, $p_t > 20\,\mathrm{MeV}/c$	31	118	47	425
Minijet ev./100 ns, $p_T^{\min} = 3.2\,\mathrm{GeV}/c$	.003	.017	.016	.16
Physics events per hour				
Bhabha	3200	3000	900	1000
W^+W^-	140	133	34	36
$q\bar{q}$	63	60	19	20
$t\bar{t}$	15	14	5	5
$\nu\nu H_{SM}(M_{H_{SM}} = 140\,\mathrm{GeV})$	1.4	1.4	2.9	3.0
ZH_{SM}	1.2	1.2	0.4	0.4

Table 2.1.7: *Table of some machine properties and related backgrounds.*

Bibliography

[1] *ECFA/DESY Study of Physics and Detector for a Linear Collider*, http://www.desy.de/conferences/ecfa-desy-lc96.html, proceedings to be published as DESY 97-123E.

[2] *Proceedings of the Workshop on Physics at Future Accelerators*, La Thuile 1987, ed. J.H. Mulvey, CERN 87-07 (1987).

[3] C. Ahn et al., *Opportunities and Requirements for Experimentation at a Very High Energy e^+e^- Collider*, SLAC-Report-329 (1988).

[4] *Proceedings of the Summer Study on High Energy Physics in the 1990s*, Snowmass, 1988, ed. S. Jensen, World Scientific, Singapore, 1989.

[5] Three Workshops on the Japan Linear Collider (1989,1990,1992) resulting in: JLC Group, *JLC-I*, KEK Report 92-16 (1992). The latest workshop took place in 1995.

[6] *e^+e^--Collisions at 500 GeV: The Physics Potential, Parts A and B*, Workshops at Munich, Annecy, Hamburg, 1991, ed. P.M. Zerwas, DESY 92-123A&B (1992).

[7] *Physics and Experiments with Linear Colliders, Vols. I and II*, eds. R. Orava, P. Eerola and M. Nordberg, World Scientific, Singapore, 1992.

[8] *Proceedings of the 1992 Workshops on High-Energy Physics with Colliding Beams*, Trilogy of Workshops at Yale, Wisconsin, Santa Cruz, 1992, ed. J. Rogers, SLAC-428 (1993).

[9] *Workshop on Physics and Experiments with Linear e^+e^- Colliders, Vols.I and II*, Waikoloa, Hawaii, 1993, eds. F.A. Harris, S.L. Olsen, S. Pakvasa and X. Tata, World Scientific, Singapore, 1993.

[10] *e^+e^--Collisions at 500 GeV: The Physics Potential, Part C*, Workshops at Munich, Annecy, Hamburg, 1992-1993, ed. P.M. Zerwas, DESY 93-123C (1993).

[11] D.Burke, "Status of the Interregional Collaboration", Opening Session at the *Fifth International Workshop on Next-Generation Linear Colliders*, (LC93, SLAC, October 13-21, 1993), SLAC-436 (1993).

[12] *Proceedings of the Zeuthen Workshop on Elementary Particle Theory – Physics at LEP200 and Beyond*, Teupitz/Brandenburg, Germany, April 1994, eds. T. Riemann and J. Blümlein, Nucl. Phys. B (Proc. Suppl.) 37B (1994).

[13] *Proceedings of the Gamma-Gamma Collider Workshop* Berkeley, March 28-31, 1994, ed. A. Sessler, Nucl. Instr. and Meth. A355 (1995).

[14] *Proceedings of the Santa Cruz Workshop on* $\mathrm{e^-e^-}$ *Collisions*, Sept. 4-5, 1995, ed. C. Heusch, to be published.

[15] *Physics with* e^+e^- *Linear Colliders, Part D*, Workshops at Annecy, Gran Sasso, Hamburg, 1995, ed. P.M. Zerwas, DESY 96-123D.
Members of the working group on experimentation were: P. Bambade, W. Bartel, T. Benke, G. Blair, T. Bolognese, A. Bonissent, R. Brinkmann, J. Bürger, O. Callot, G. Coignet, P. Comas, G. Cowan, M. Danilov, P.-G. Denis, E. Elsen, M. Grünewald, D. Haidt, J.D. Hansen, J. Harton, P. Hüntemeyer, L. Jönsson, F. Kapusta, S. Katsanevas, D. Kisielewska, U. Kötz, S. Komamiya, A. Lebedev, M. Leenen, B. Löhr, K. Long, P. Mättig, J. Meyer, D. Miller, J. Milewski, R. Miquel, A. Olshevski, K. Piotrzkowski, M. Pohl, F. Richard, A. Rousarie, E. Rulikowska, H.-G. Sander, M. Schmelling, M. Schmitt, U. Schneekloth, H.-J. Schreiber, S. Schreiber, D. Schulte, R. Settles, S. Shuvalov, A. Sopczak, P. Steffen, H. Steiner, L. Suszycki, T. Tauchi, J. Thompson, I. Typakin, A. Venturi, H. Videau, A. Wagner, R. Walczak and G.W. Wilson.

[16] *Proceedings of LCWS95, the 1995 International Linear Collider Workshop at Morioka-Appi*, Sept. 8-12, 1995, World Scientific, 1996.

[17] R. Settles, et al., *Experimentation at the Linear Collider*, in Ref. [16].

[18] *International Linear Collider Technical Review Committee Report 1995*, Stanford Linear Accelerator Center Technical Publications Department, order number SLAC-R-95-471, G. Loew/SLAC(Chair) and T. Weiland/TH Darmstadt (Secreteriat).

[19] The proceedings of the studies in the USA by "DPF Long Range Planning" working groups (DPF is the Division of Particles and Fields of the American Physical Society), available on the World Wide Web under http://fermi.pha.jhu.edu/dpf/cltp/index.html

[20] D.J. Miller, *Other Collider Options*, in Ref. [16]; see Appendix A to this Conceptual Design Report.

[21] J.M. Baze, H. Desportes et al., “Design, Construction and Test of the Large Superconducting Solenoid ALEPH”, IEEE Trans. on Magnetics, Vol. 24, March 1988, p. 1260-63.

[22] “The Compact Muon Solenoid (CMS) technical proposal”, CERN/LHCC 94-38, LHC/P1.

[23] P. Colas, F.P. Juster, F. Kircher, “Concepts for a detector magnet for linear e^+e^- collider experiments”, CEA report, to be published.